Atomic-scale investigations of isothermally formed bainite microstructures in 51CrV4 spring steel

Goulas, Constantinos; Kumar, Ankit; Mecozzi, Maria Giuseppina; Castro-Cerda, Felipe Manuel; Herbig, Michael; Petrov, Roumen H.; Sietsma, Jilt

DOI
10.1016/j.matchar.2019.03.038

Publication date
2019

Document Version
Final published version

Published in
Materials Characterization

Citation (APA)
Goulas, C., Kumar, A., Mecozzi, M. G., Castro-Cerda, F. M., Herbig, M., Petrov, R. H., & Sietsma, J. (2019). Atomic-scale investigations of isothermally formed bainite microstructures in 51CrV4 spring steel. *Materials Characterization*, *152*, 67-75. https://doi.org/10.1016/j.matchar.2019.03.038

Materials Characterization 152 (2019) 67–75

Contents lists available at ScienceDirect

Materials Characterization

journal homepage: www.elsevier.com/locate/matchar

Atomic-scale investigations of isothermally formed bainite microstructures in 51CrV4 spring steel

Constantinos Goulas[a,b,*], Ankit Kumar[b,c,d], Maria-Giuseppina Mecozzi[b], Felipe Manuel Castro-Cerda[e], Michael Herbig[d], Roumen H. Petrov[b,c], Jilt Sietsma[b]

[a] Materials innovation institute (M2i), Electronicaweg 25, 2628XD Delft, the Netherlands
[b] Delft University of Technology, Department of Materials Science and Engineering, Mekelweg 2, 2628CD Delft, the Netherlands
[c] Gent University, Department of Materials Science and Engineering, Technologiepark 903, 9052 Zwijnaarde, Gent, Belgium
[d] Max-Planck-Institut für Eisenforschung, Max-Planck-Strasse 1, 40237 Düsseldorf, Germany
[e] Department of Metallurgical Engineering, Universidad de Santiago de Chile, Av. Lib. Bdo. OHiggins 3363 Estacion Central, Santiago de Chile, Chile

ARTICLE INFO

Keywords:
Bainite
Atom probe tomography
Transmission electron microscopy
Spring steel

ABSTRACT

Atomic-scale investigation was performed on 51CrV4 steel, isothermally held at different temperatures within the bainitic temperature range. Transmission electron microscopy (TEM) analysis revealed three different morphologies: lower, upper, and inverse bainite. Atom Probe Tomography (APT) analysis of lower bainite revealed cementite particles, which showed no evidence of partitioning of substitutional elements; only carbon partitioned into cementite to the equilibrium value. Carbon in the bainitic ferrite was found to segregate at dislocations and to form Cottrell atmospheres. The concentration of carbon remaining in solution measured by APT was more than expected at the equilibrium. Upper bainite contained cementite as well. Chromium and manganese were found to redistribute at the cementite-austenite interface and the concentration of carbon in the ferritic matrix was found to be lower than the one measured in the case of lower bainite. After isothermal treatments close to the bainite start temperature, another austenite decomposition product was found at locations with high concentration of Mn and Cr, resembling inverse bainite. Site-specific APT analysis of the inverse bainite reveals significant partitioning of manganese and chromium at the carbides and at the ferrite/martensite interfaces, unlike what is found at isothermal transformation products at lower temperatures.

1. Introduction

The formation of bainite has been attracting scientific interest for almost a century. What makes it attractive is the fact that it combines characteristics of fundamentally different phases, which are martensite and Widmanstätten ferrite; this circumstance is the reason why the mechanism of formation of this phase, a mixture of ferrite and cementite, is still object of controversy. The morphology of ferrite and the distribution of carbides depend on the transformation temperature and therefore bainite is usually classified as either upper bainite or lower bainite. When formed at low temperatures, lower bainite shares common characteristics with martensite and it is sometimes even impossible to distinguish them microscopically. This experimental finding suggests that the mechanism of formation of bainite is similar to that of martensite and therefore might be diffusionless in nature. On the other hand, an increasing number of experimental and theoretical studies support the similarity between bainitic ferrite and proeutectoid ferrite with Widmanstätten morphology and the idea that bainite growth is determined by carbon diffusion.

Hultgren first proposed in 1947 that upper bainite could form by initial precipitation of ferrite with Widmanstätten morphology followed by cementite precipitation on its sides [1]. The concept was further analysed by Hillert, who has shown that there is no reason to treat Widmanstätten ferrite and bainitic ferrite as different products, as there is no kinetic discontinuity [2]. According to this approach, the bainitic ferrite nucleates at austenite grain boundaries and grows at a rate determined by the diffusivity of carbon. Aaronson et al., supporting the above-described theory, have considered the effect of alloying elements on the bainitic transformation, and the potential segregation of substitutional elements at the growing phase interface [3].

The diffusionless approach to bainite formation was introduced by Zener in 1946 [4], further developed by Ko and Cottrell [5], and more recently supported by Bhadeshia [6]. According to this approach, a subunit of bainitic ferrite, supersaturated in carbon, nucleates on an

* Corresponding author at: Materials innovation institute (M2i), Electronicaweg 25, 2628XD Delft, the Netherlands
E-mail address: k.goulas@tudelft.nl (C. Goulas).

https://doi.org/10.1016/j.matchar.2019.03.038
Received 5 February 2019; Received in revised form 22 March 2019; Accepted 24 March 2019
Available online 29 March 2019
1044-5803/

austenite grain boundary. The growth is instantaneous and displacive and stops because of the plastic deformation of the adjacent austenite. The bainitic ferrite is initially supersaturated with carbon, which needs to be rejected by diffusion into the residual austenite, in which it can form carbides with para-equilibrium composition. Carbon can also directly precipitate in the form of carbides within the bainitic ferrite sub-unit, if insufficient diffusion can take place due to the transformation temperature being low. Once bainitic sub-units have formed, the bainite formation can continue by the autocatalytic nucleation and displacive growth of new sub-units on the tip of previously formed sub-units.

Recent studies have revealed that, although carbon is depleted from bainitic ferrite, bainitic ferrite even after long times retains more carbon than is theoretically predicted by thermodynamic equilibrium. Recent Atom Probe Tomography and Synchrotron X-Ray Diffraction studies observe this phenomenon and some authors claim that the carbon that is trapped in the bainitic ferrite causes tetragonality of its cubic lattice [7–8]. However, the fact that the carbon does not diffuse out of the bainitic ferrite given the time and the driving force still cannot be explained satisfactorily.

The composition appears to be playing a very important role in the morphology of bainite. Especially in high carbon and chromium containing steels, when austenite decomposes at temperatures between 500 and 700 °C, non-classical austenite decomposition products were reported. One of them, formed close to the bainite start temperature (around 500 °C), is called inverse bainite on the basis of its inverse morphological characteristics with respect to the conventional bainite [9]. Inverse bainite is in fact identified as a phase mixture of carbide plates surrounded by Widmanstätten ferrite. The presence of inverse bainite was used by Borgenstam et al. to support the concept that austenite decomposition occurs by “mirror mechanisms” for compositions lower and higher than the eutectoid composition [10], and thus claim the generality of the diffusional mechanism in bainite formation. By mirror mechanisms it is implied that bainite and inverse bainite are products of austenite decomposition, which are obtained by similar processes, but with their constituents, ferrite and cementite, having opposite roles. In a bainitic microstructure, a leading phase grows from the prior austenite grain boundary with a Widmanstätten morphology, followed by the formation of a secondary phase. Following this mechanism, at hypo-eutectoid compositions, the leading phase is ferrite, while at hyper-eutectoid compositions the leading phase is cementite. Recent studies on inverse bainite formation have more clearly defined its mechanism in terms of thermodynamics and have provided insight into the microstructural and crystallographic aspects [11–12,14–16].

Besides carbon, substitutional alloying elements such as Mn, Cr, and Mo are known to affect the formation of bainite in different ways. The presence of these elements in steel retards the growth of bainite by inducing a solute drag effect and can also limit the maximum fraction of bainite that can be obtained from an isothermal treatment at a given temperature (incomplete reaction phenomenon) [11–16].

Cr addition reduces the eutectoid carbon composition of steels, so even alloys with C content as low as 0.4 wt% can produce microstructures similar to the ones found in hypereutectoid Fe—C steels. This is especially applicable to the observation of inverse bainite, which is primarily found in hyper-eutectoid steels. Recent studies reported similar microstructures in Cr containing steels with lower carbon contents [17].

Transmission Electron Microscopy (TEM) studies of inverse bainite microstructures show evidence of a crystallographic orientation relationship between the acicular carbides, the surrounding ferrite and the parent austenite. This was achieved by relating the orientation of retained austenite in partially transformed specimens with the orientation of the carbides and the ferrite sheaves.

Information about the composition of the different constituents of the inverse bainitic microstructure is very limited in literature, most of the studies report the carbides as being of the M_7C_3 type with significant partitioning of Cr from the matrix to the carbide. Detailed study on the composition of the non-classical decomposition products of austenite can help to elucidate the transformation mechanism leading to their formation, as well as the relation between these products and conventional bainite. Due to the fine scale of the microstructure, a high resolution chemical composition analysis technique is required. Atom Probe Tomography (APT) is a very suitable technique for such an analysis, especially if combined with site-specific tip preparation and TEM. In this work, the microstructures obtained by isothermal treatment of 51CrV4 steel within the temperature range of bainite formation are studied by means of transmission electron microscopy and atom probe tomography. TEM provides information about the bainitic microstructure morphology at different temperatures, APT enables a detailed compositional analysis of these microstructures. The compositional information can help elucidate the reasons for the wide morphological variety of bainite in medium carbon low alloy steel grades.

2. Experimental procedure

Samples of 51CrV4 steel were received in as rolled condition. The samples were cut out from hot rolled bars with dimensions $95 \times 49 \times 5500\,mm^3$. The chemical analysis was performed on $30 \times 30\,mm^2$ cross-sections of the bars, perpendicular to the rolling direction, by means of Optical Emission Spectroscopy (OES). The chemical composition of 51CrV4 steel is shown in Table 1.

Besides the average chemical composition, local fluctuations in the chemical composition, expected to affect the phase transformations, were measured in the normal direction by Electron Probe Micro Analysis. The details of the measurement, as well as the interpretation of the effect of the segregation on the microstructure formation were previously published by the authors [17]. The concentration profile of Cr and Mn is shown in Fig. 1.

The dilatometric specimens with dimensions $\Phi 4 \times 10\,mm^2$ were machined using Wire Electro-Discharge Machining (EDM). The dilatometric tests were performed in a Bähr 805A Quench dilatometer, with the heat treatment schemes shown in Fig. 2. The specimens were placed in the dilatometer with two thermocouples, spot welded, one at the centre and the other 1 mm from the edge in order to control the temperature and observe its gradient during the treatment. All samples were heated within 60 s to the austenitisation temperature (900 °C) under vacuum and then quenched to an isothermal holding temperature in the range 300–510 °C using helium gas. After the isothermal holding, the samples were quenched to room temperature. The quenching rate was high enough to avoid austenite-to-ferrite transformation according to TTT diagrams for the specific chemical composition. This rate was chosen to be 30 °C/s.

For microstructural characterization, dilatometric samples were mounted on a specially designed sample holder, then ground, polished and etched with Nital 2%. Scanning Electron Microscopy (SEM) analysis was carried out in a Field Emission Gun Scanning Electron Microscope (FEG-SEM) JEOL 6500F operated at 15 kV. For TEM analysis, specimens were prepared from the dilatometry samples after austenitisation and isothermal holding. Although the temperature gradient within the dilatometric specimen during the heat treatment was found to be within 10 °C, in order to ensure that the microstructure observations were consistent with the dilatometry measurements, the sample discs were cut from the central zone of the dilatometric

Table 1
Chemical composition of the 51CrV4 grade as measured by Optical Emission Spectroscopy.

Elements	C	Mn	Si	Cr	V
Wt%	0.51	1.02	0.33	1.15	0.12
At.%	2.32	1.01	0.64	1.21	0.13

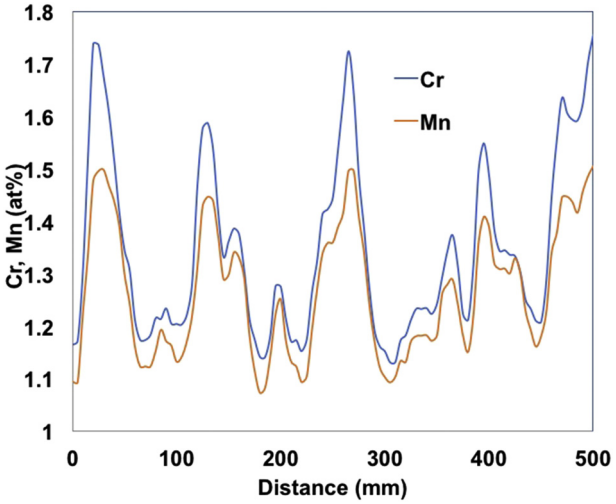

Fig. 1. Concentration profile of Mn and Cr as measured with EPMA.

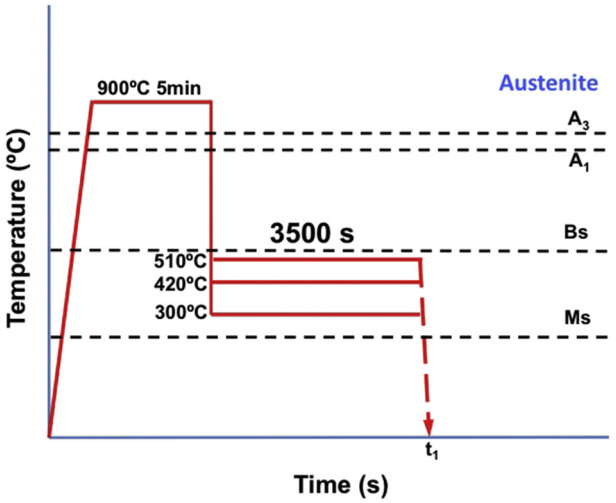

Fig. 2. Heat treatment schemes used in the dilatometer.

specimen, close to the thermocouple. The TEM discs were manually ground down to 60 μm, and then Ar-ion polished to final electron transparent thickness using a GATAN 691 PIPS system. For the observation, a JEOL JEM-2100 electron microscope operated at 200 kV was used.

APT samples were also prepared from the dilatometry specimens using focused Ion Beam (FIB) milling. Lift-out procedures, as described in Ref. [18–20] were used to produce the atom probe specimens. The method as described in [19] is employed for APT sample preparation to study the acicular cementite in inverse bainite. Its size on the order of tens of nanometres and its non-uniform distribution in the microstructure made it particularly challenging to capture inverse bainite within an APT specimen, using the conventional lift out procedure. Thus, the method applied in the present study incorporated as a first step coarse FIB cutting at 52° and 0° sample tilt. The FIB-cut lamella was then placed at an axial manipulator and rotated 90° manually after opening the FIB chamber as shown in Fig. 3. After rotation, the lamella was lifted out from the axial manipulator and then welded using platinum on electro-polished molybdenum posts [21].

APT measurements were performed using a local electrode atom probe (LEAP 3000X HR, Cameca Instruments) in voltage mode at a specimen temperature of −213 °C (60 K). The pulse fraction and the pulse frequency were 15% and 200 kHz, respectively, for all measurements. APT data analysis was performed using the IVAS software (Cameca Instruments). Calibration of the Image Compression Factor (ICF) and K_f constant as per the procedure explained in [22–23]. A peak decomposition algorithm incorporated in the IVAS software was used to decompose the ($12C_3 13C^{2+}$) peak at a mass-to-charge ratio of 24.5 Da.

3. Results

3.1. Isothermal treatment at 300 °C

The isothermal treatment at 300 °C, despite the macro-chemical segregation detected by EPMA, produced a homogeneous bainitic microstructure after 1 h of treatment. Fig. 4a shows the bainitic microstructure produced after 1 h holding at 300 °C. Extensive carbide precipitation is evident. The carbides are fine and elongated, aligned at an angle towards the length of the bainitic ferrite plate.

For observation at a higher magnification, TEM was employed. The observation in the TEM confirms the presence of elongated carbides parallel to each other within the ferrite plates. No carbides are found at the plate boundaries (see Fig. 4b). Significant presence of dislocations is verified in the specimen and their distribution appears to be homogeneous.

In order to obtain compositional information about the carbides and the bainitic ferrite, APT tips were obtained from an area containing both bainitic ferrite and carbides by site specific preparation.

In Fig. 5, the reconstructed APT ion maps of C, Cr, Mn and Si are shown. It is evident from the C map that in the analysed volume two large carbon clusters are present. The two large clusters are around 60 nm apart and parallel to each other, resembling the carbides observed in TEM in lower bainite, Fig. 4b. In between those clusters there are numerous smaller C accumulations without showing clearly defined shapes. The maps of Cr and Mn in the analysed areas do not show any signs of partitioning between ferrite and cementite. Fig. 5b. However, Si appears to be the only alloying element that shows concentration difference across the bainitic ferrite/carbide interface. There is slight accumulation of Si of approximately 1.2 at.% at the interface.

Quantitative chemical information can be obtained by the proximity histograms. Fig. 5b shows the proximity histogram of the lower large C cluster with the zero position at an isosurface of 25 at.% C. The proximity histogram shows a carbon content of around 25 at.% in the centre of the carbide. Indeed, there is no partitioning of Cr or Mn. The last point of the Cr measurement appears to be high, but the error of this point is high as well, so it can be concluded that there is no significant Cr fluctuation within the carbide. The reduced concentration of Si in the carbides and its increased concentration around the α/θ interface is verified by several measurement points with very limited error margin. The above analysis shows that the carbides formed at 300 °C can be identified as cementite formed under non-partitioning conditions for the substitutional elements (cementite in para-equilibrium conditions), with the Si most probably partitioning during isothermal holding, after carbide formation.

In order to analyse the smaller carbon clusters observed in the areas between two adjacent carbides, C isosurface maps were constructed at carbon concentrations between 4 and 11 at.%, Fig. 6. This analysis shows that carbon accumulates in three dimensional features, while the other elements do not redistribute. The carbon concentration at these features reaches 11 at.%. The same analysis was performed for the bulk of the bainitic ferrite, this time excluding areas with a carbon content higher than 1 at.%. In this way, the carbon content in solution in the matrix was estimated. The result shows that the carbon concentration in the matrix is on average 0.65 at.%, higher than the equilibrium value 0.27 at.%, determined from the α/γ line in the phase diagram, calculated with Thermocalc and extrapolated to 300 °C.

3.2. Isothermal treatment at 420 °C

In contrast to the isothermal treatment at 300 °C, the treatment at

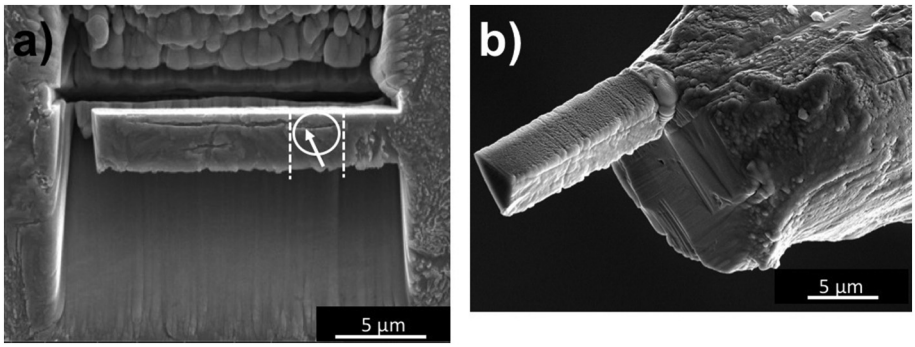

Fig. 3. Site specific FIB milling of the APT tips. a) SEM micrograph from the location of the site-specific Atom Probe Tomography tip preparation by FIB and b) rotation of the lamella by 90° with an axial manipulator to have the region of interest close to the atom probe tip (circle with arrow showing the annular milling direction, dashed lines show the cut area of the specific tip).

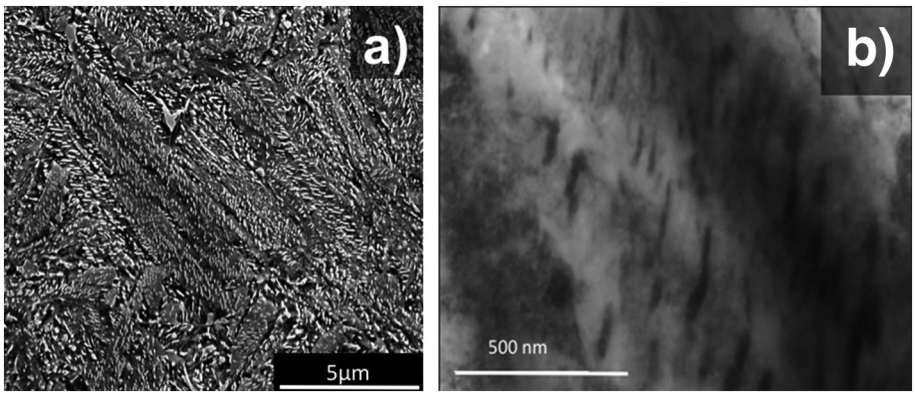

Fig. 4. a) SEM Micrograph showing bainitic microstructure obtained after isothermal holding at 300 °C for 1 h. b) Bright Field Transmission Electron microscopy micrograph showing typical morphological characteristics of lower bainite.

420 °C did not produce a homogeneous microstructure. The SEM micrographs show that there are areas in the microstructure that transformed into bainite, with distinct features evident after the etching, but other areas remain featureless. The featureless areas can be identified as martensite/austenite islands (M/A), and they form during the final quenching from the isothermal treatment temperature to room temperature, Fig. 7a. The M/A areas contain high concentrations of Cr, Mn and Si. The morphology of bainite after isothermal treatment at 420 °C is different from the one found at 300 °C. The shape of the bainitic ferrite plates is not acicular; the carbides are coarser and are found at the platelet boundaries.

TEM observation provides information at higher magnification, Fig. 7b. The matrix is coarser and shows some granular sub-structure. Dislocations are evident, but there are areas with clearly lower density of dislocations. The carbides are coarser and more elongated than in the case of bainite formed at 300 °C.

Fig. 8a shows the ion maps for C, Cr, Mn and Si. The C-map reveals two large carbon clusters and a low-carbon matrix, whereas the maps of substitutional elements show a slight enrichment at the interface of the carbides. Fig. 8b shows the proximity histogram plotted from a C isosurface of 25 at.%. The proximity histogram shows that the carbon content of the carbide is around 25 at.% in the interior of the particle, but also that there is a slight increase of Cr and Mn content close to the interface. In contrast, the silicon is depleted from the interior of the carbide to the interface, where Si content reaches a maximum of 1.2 at.%, with the composition inside the carbide being around 0.33 at.%. The APT results suggest that the carbides forming under these conditions are also cementite, which can be enriched slightly in Cr and Mn and depleted in Si.

The carbon content of the bulk was measured in this sample

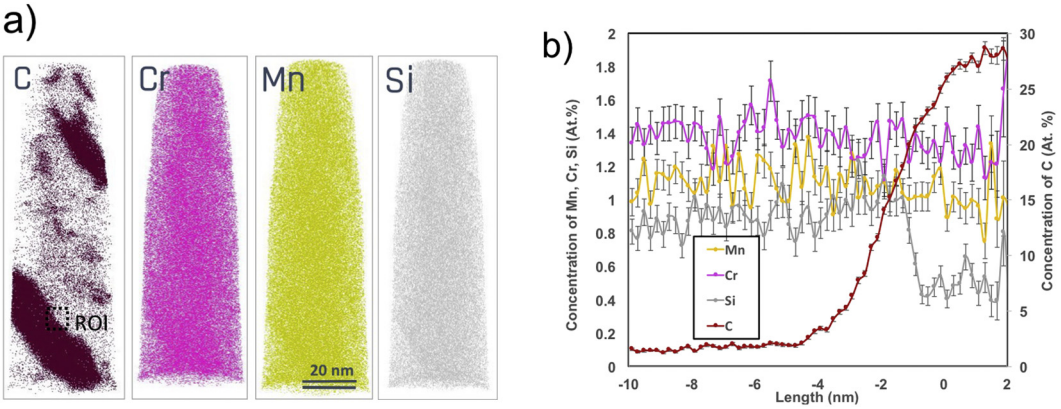

Fig. 5. a) APT Ion maps of C, Cr and Mn from a sample that was isothermally transformed into bainite at 300 °C. The C map reveals two cementite particles and C clustering in bainitic ferrite. b) Proximity histogram of the lower carbide, taken in the Region Of Interest (ROI) indicated in the C map of a), showing no partitioning of Cr and Mn. The Si concentration is reduced in the cementite.

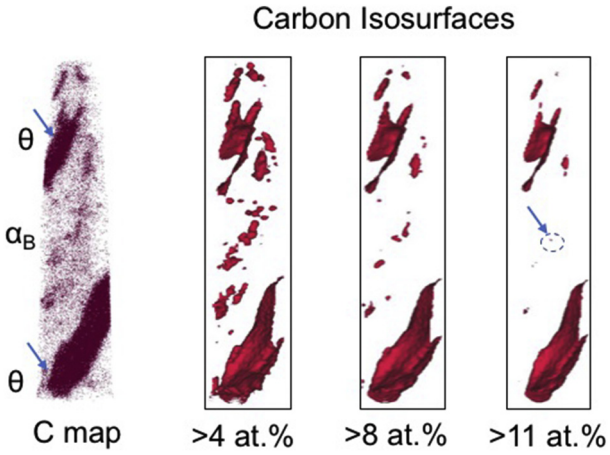

Fig. 6. APT carbon ion map and carbon isosurfaces of 4 at.%, 8 at.% and 11 at. %, bainite isothermally formed at 300 °C. In between the two large carbides, smaller carbon clusters are found in the sample.

following the same procedure. The results indicate that the carbon content in ferrite of upper bainite is 0.35 at.%, higher than the equilibrium value resulting from the extrapolated α/γ line in the phase diagram at the selected temperature, calculated by Thermocalc, which is 0.12 at.%.

3.3. Isothermal treatment at 510 °C

The specimens that were isothermally treated at 510 °C differed fundamentally from the ones transformed at lower temperatures, Fig. 9. The microstructure characterization reveals multiple microstructural constituents. Allotriomorphic ferrite with Widmanstätten secondary plates are evident at prior austenite grain boundaries. Additionally, an aggregate of acicular carbides surrounded by thin layers of ferrite is found to grow directionally from the α/γ interface, coinciding with the prior austenite grain boundaries, Fig. 9a. In the areas surrounding these aggregates, the microstructure remains unetched, and these areas are identified as M/A resulting from the final quench to room temperature. This is consistent with the observation that the isothermal treatment was interrupted before the transformation was complete.

The TEM analysis of this microstructure focused on the carbide-ferrite aggregates, in order to elucidate the formation mechanism. Bright-Field (BF) TEM micrographs show that the carbides have a needle or fibre morphology. They are generally surrounded by a film of ferrite, but occasionally carbides are found to be directly surrounded by martensite, as indicated by the arrows in Fig. 9b. The martensite is characterized by its different contrast, which indicates higher dislocation density, aided by Selected Area Electron Diffraction (SAED). The carbides are identified to be cementite by means of SAED and Dark Field imaging from $(\bar{3}\bar{1}\bar{1})$ reflection of cementite, Fig. 9c–d. The thickness of the carbides is around 10 nm, while the thickness of the surrounding ferrite is consistently measured to be around 20–30 nm. The aggregates exhibit a certain degree of branching, at an angle of around 60° from the main direction of the aggregate.

The APT elemental maps show multiple areas, in which redistribution of C, Mn, Cr, and is evident, Fig. 10a. There is an area clearly defined by two interfaces enriched in C, Mn and Cr, which outlines the carbide-ferrite aggregate detected in TEM. Within the aggregate, the ferrite film is depleted from C, Cr, Mn and enriched in Si. Approaching the ferrite/carbide interface, the Si concentration reaches a peak and the concentration of C, Cr and Mn gradually increase. Finally, within the cementite, C reaches a peak concentration of around 21 at.%, with the Cr concentration being around 8 at.% and the Mn concentration around 5 at.%, Fig. 10b. The θ/α interfaces are significantly enriched in C, Mn, and Cr and depleted of Si as well, as seen by the proxigram in Fig. 10b.

4. Discussion

4.1. Lower bainite (300 °C)

After isothermal transformation at 300 °C, the microstructure is homogeneous at the micro-scale, which means that the sample contains areas that transformed into bainite while containing high Cr, Mn, and Si concentrations. In this particular case, it is interesting to measure the composition of the bainitic ferrite and the carbides in order to examine the possible effect of Cr, Mn and Si on the evolution of the transformation. Therefore, for the sample preparation, the bulk composition of the area was chosen to contain a high concentration of alloying elements, so in case alloying element re-arrangement would occur, it would be evident in the measurement.

APT carbon maps reveal two precipitates with around 25 at.% of carbon, Fig. 5. Cr and Mn maps show no redistribution of these elements between the precipitate and the ferritic matrix. Si, on the other hand, is found to have a lower concentration inside the precipitate. Since the isothermal treatment is 1 h long and the exact time of the formation of the specific carbides is not known, we assume that Si, similarly to the other substitutional alloying elements present in the sample, did not partition during the formation stage, as it is also claimed for the case of cementite formation in tempered martensite at similar temperatures [24]. Given the fact that the diffusivity of Si in α iron is higher than the the diffusivities of Cr and Mn at 300 °C [25], it is suggested that the redistribution of Si occurred after the precipitation, during the holding at 300 °C. The depletion of silicon from the precipitates and the accumulation of this element at the precipitate's interface with bainitic ferrite can contribute to the retardation of carbide growth during further isothermal holding [25]. In this framework, the

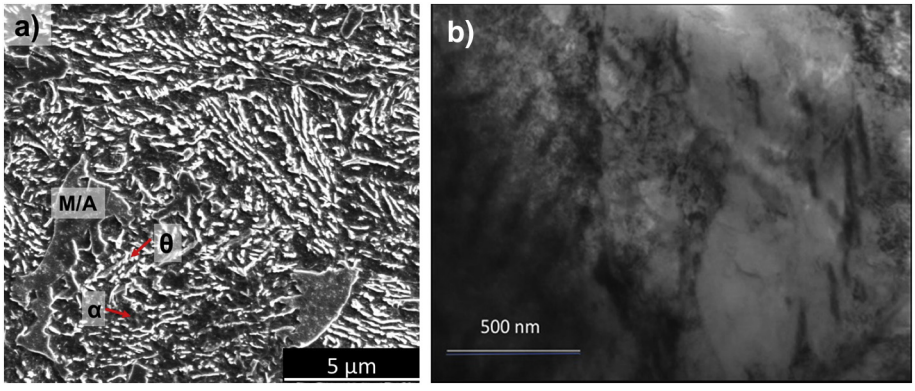

Fig. 7. a) SEM micrograph showing upper bainitic microstructure obtained after heat treatment at 420 °C. b) Bright Field TEM micrograph of the same specimen.

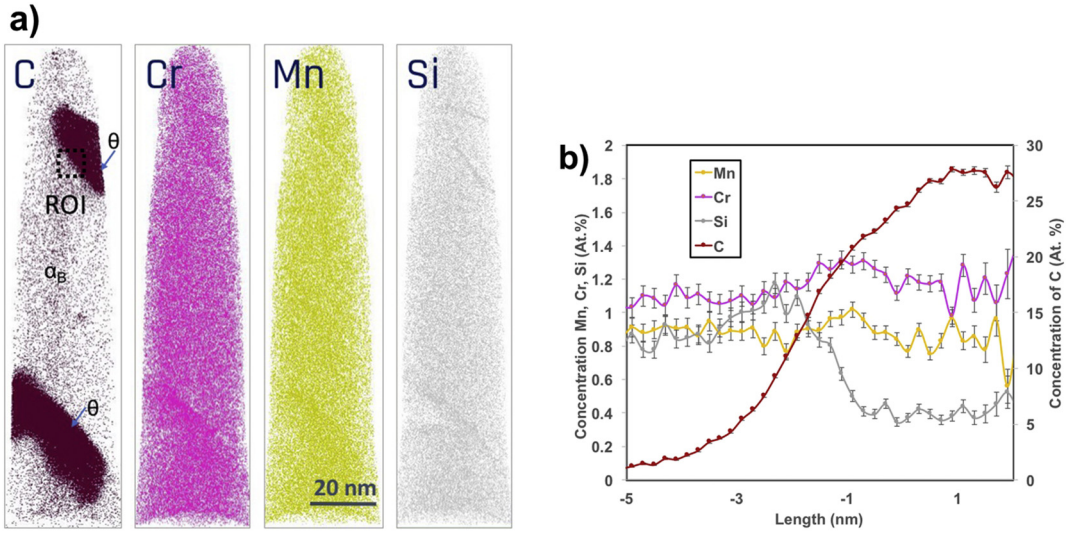

Fig. 8. a) APT Ion maps of C, Cr and Mn of a specimen isothermally transformed into upper bainite at 420 °C. The C maps show two cementite precipitates. There is no C agglomeration at locations apart from the cementite. b) Proxigram of the upper cementite particle shown in a). Cr and Mn exhibit slight partitioning into the cementite, and Si is depleted from the cementite to the surrounding bainitic ferrite. The profile is taken normal to the interface between cementite-ferrite (positive values inside cementite in the ROI indicated in the C map of figure a)).

time of the treatment after the precipitation of the carbides has an effect on the microstructure that is similar to tempering. As far as the other substitutional alloying elements are concerned, there is no difference of their concentrations in the carbides and in the bainitic ferrite.

Furthermore, carbon clusters are observed in between the precipitates. Using carbon isosurfaces, Fig. 6, it is shown that these clusters reach concentrations higher than 11 at.% of carbon. The carbon concentration of these clusters is more than the value of 6–8 at.% reported in literature for Cottrell atmospheres, formed by segregation at the dislocations [27]. However, the concentration is less than expected for transitional carbides or cementite. Given the fact that, according to TEM observations and literature [27], the dislocation density is high for the bainitic ferrite, carbon is expected to segregate at dislocations. Other studies [26] show that close to the precipitates and at the grain

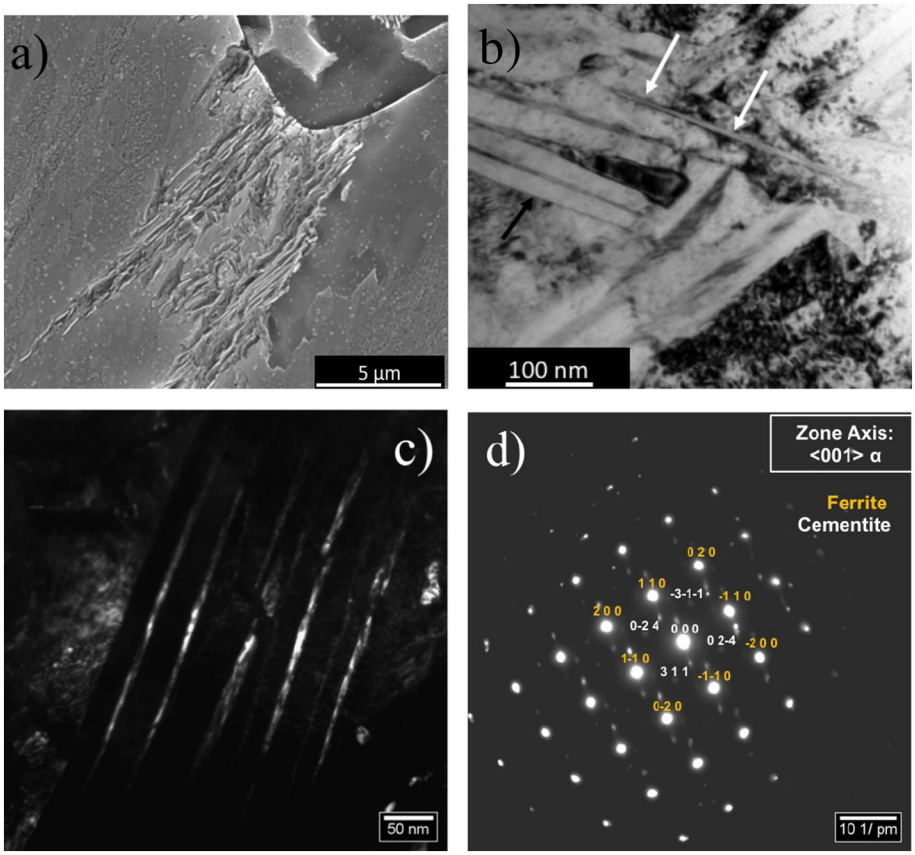

Fig. 9. a) SEM micrograph showing the microstructure obtained after isothermal holding at 510 °C for 1 h. b) Corresponding Bright Field TEM micrographs of the same specimen. c) Dark Field image obtained from the ($\bar{3}\bar{1}\bar{1}$) reflection of cementite d) SAED Pattern of ferrite and cementite, zone axis: < **001** > ferrite.

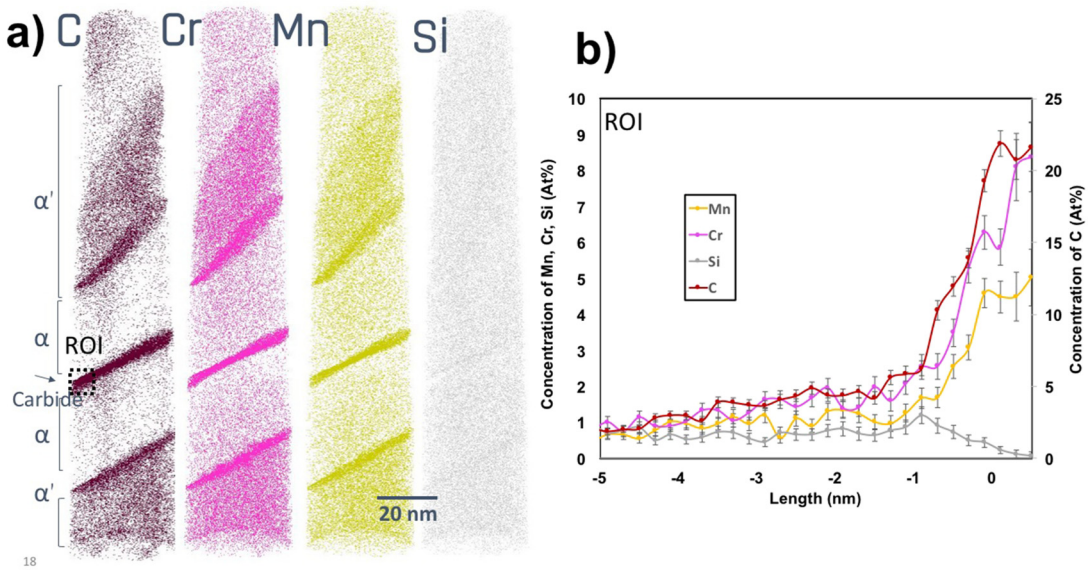

Fig. 10. APT ion maps of C, Cr, Mn, and Si of a sample isothermally transformed at 510 °C for 1 h. Significant redistribution of all elements studied is evident. b) Proximity histogram for the Region Of Interest indicated in figure a). The proximity histogram profile showsis taken normal to the concentrationinterface between cementite-ferrite (positive values inside cementite).

boundaries there is an increase in dislocation density and carbon tends to get trapped at such lattice defects. Carbon clusters were found to be located in between the two precipitates, which could be attributed to an increased dislocation density at these locations. The dislocation density could be high at that location due to high transformation strain accommodation by the bainitic ferrite.

The high carbon concentration observed in the matrix (equal to 0.65 at.%) is consistent with observations of previous studies using APT [26] or synchrotron techniques [7,8]. An explanation for the increased carbon solubility in bainitic ferrite has been proposed by Hulme-Smith et al. [8], who support the hypothesis that the higher carbon content observed in ferrite is a consequence of an increased carbon solubility due to the change in symmetry from the conventional cubic unit cell to the tetragonal unit cell. The present observations do however not reveal information on the tetragonality of the bainitic ferrite.

4.2. Upper bainite (420 °C)

In upper bainite, the results show that the transformation produces cementite, but in this case some partitioning of Mn and Cr is observed at the cementite-ferrite interface. This trend is consistent with previous observations by APT [24–25] performed on martensitic samples, tempered at similar temperature range.

As far as the bainitic ferrite matrix is concerned, there is no carbon segregation inside the ferrite region between the two adjacent cementite particles. This is in agreement with TEM observations showing a lower dislocation density in bainite formed at 420 °C (Fig. 6b). The dislocation density in upper bainite, although it was not directly measured or calculated, it can be expected to reach values of the order of 10^{13} m^{-2}. This assumption is based on the dislocation density value calculated by using tensile test data in tempered martensite sample, as it was explained in Chapter 5 of [28], and on TEM analysis showing that the bainitic ferrite matrix in upper bainite resembles the one of martensite tempered at 480 °C in terms of contrast.

The APT tips from this specimen were prepared using site-specific preparation. In this case, choosing an area of strong segregation of Mn and Cr for the analysis was not relevant, since these areas do not transform into bainite. Thus, the tips were prepared from a transformed area, which contained carbides.

4.3. Inverse bainite (510 °C)

The SEM micrograph of Fig. 9a shows that the cementite is always found to nucleate at prior austenite grain boundaries. In previously published research of the authors, it was shown that this cementite is forming in bands where high concentrations of Mn and Cr are found. This segregation implies that the local thermodynamic conditions are different from for the rest of the material, and the austenite decomposition at these locations will follow a different sequence, as shown in Fig. 6 of [17]. The austenite in Cr-rich and Mn-rich regions will decompose following the phase formation sequence of hyper-eutectoid steels [29]. It has been reported in such cases that the so-called inverse bainite can be formed. This type of ferrite and cementite phase mixture is forming with cementite directly precipitating at the austenite grain boundary, initiating the transformation. Ferrite subsequently forms surrounding the cementite. In fact, thermodynamic calculations reveal that the addition of substitutional elements in an Fe—C system changes the range of stability of different phases. The phase diagram isopleths of 51CrV4, shown in Fig. 6 of [17] for the local composition measured by EPMA at regions with high Mn and Cr segregation, reveals a eutectoid composition of 0.4 wt% C (1.8 at.%). Therefore, in the high Mn and Cr region the austenite of the investigated steel can decompose by forming pre-eutectoid cementite or M_7C_3 before forming ferrite. Carbides can be found, which are directly surrounded by martensite, without any intermediate ferrite layer, which indicates that the carbides form before the ferrite and thus can act as leading phase for the formation of this microstructure. These facts indicate that the microstructural product formed at temperatures between the temperatures for upper bainite and pearlite formation can be inverse bainite, as was reported for the higher carbon steels in literature [30–32].

Chromium has a special role in the formation of this non-classical structure. It is mainly responsible for the observed shift of the eutectoid composition to lower carbon contents; it significantly retards the bainite formation and it is found to partition in carbides. A solute drag effect can explain the retardation of bainite growth at high temperatures. The requirement for Cr diffusion for the formation of carbides explains the slow reaction kinetics of this transformation.

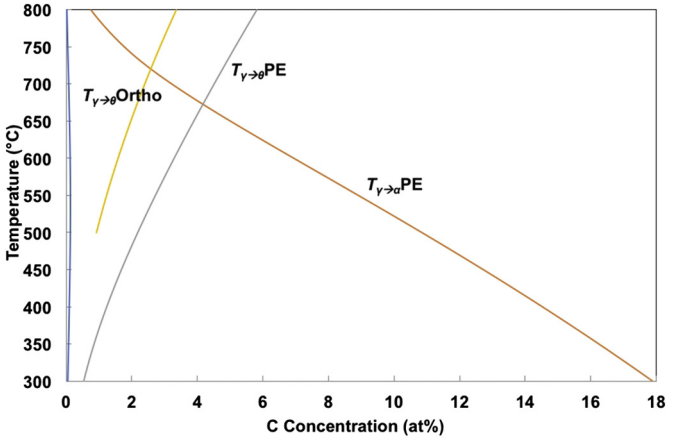

Fig. 11. $T_{\gamma\to\theta}$ and $T_{\gamma\to\alpha}$ lines under para-equilibrium conditions and $T_{\gamma\to\theta}$ line under ortho equilibrium conditions extrapolated to low temperatures.

4.4. Thermodynamic considerations - formation mechanism

The morphological and the chemical diversity observed can be further interpreted in terms of thermodynamics. Thermodynamic calculations were performed using ThermoCalc software with TCFE7 database. The $\alpha/\alpha + \gamma$ and $\gamma/\alpha + \gamma$ boundary lines were calculated in the para-equilibrium condition in the range of 600–800 °C and then extrapolated to lower temperatures. In Fig. 11 the para-equilibrium $T_{\gamma\to\theta}$ and $T_{\gamma\to\alpha}$ as well as the orthoequilibrium $T_{\gamma\to\theta}$ lines are extrapolated to lower temperatures. Based on our experimental findings, for the temperatures of 300 °C and 420 °C bainite formation can proceed under para-equilibrium conditions. However, at 510 °C, it was experimentally observed that substitutional alloying elements partition to the carbides and at segregate at the interfaces. Therefore, in this case local equilibrium conditions can be assumed, which are represented by the ortho-equilibrium $T_{\gamma\to\theta}$ line in Fig. 11.

For bainite forming at 300 °C, in TEM it was observed that there is an initial, carbide-free spine of ferrite forming without precipitation of carbides. This initial plate grows into the surrounding austenite at a rate governed by the diffusion of C. At some point, the supersaturation of C in austenite is sufficient to allow PE cementite precipitation directly from austenite at the γ/α interface according to Fig. 11. The reaction of cementite precipitation consumes the C from the remaining austenite, thus providing driving force for further grow of the bainitic ferrite without further nucleation being necessary. For bainite forming at 420 °C, the diffusivity of C is higher, hence the concentration profile at the interface is broader. The undercooling is still high enough for the transformation to occur by a shear mechanism. The higher diffusivity can explain the coarser ferrite plates and the high undercooling its morphology. The cementite in this case is also coarser, but it has another different feature: it is not aligned at a specific orientation, but it follows the γ/α plate boundaries. This happens because cementite forms at the carbon rich areas in the remaining austenite, surrounding the newly formed bainitic ferrite plates.

In the sample, isothermally treated at 510 °C, ferrite was found at the prior austenite grain boundaries, hence called allotriomorphic. However, it presented facets and sometimes acicular morphology or even degenerate Widmanstätten features. This can be attributed to the low driving force for Widmanstätten ferrite formation.

Inverse bainite formation initiates with precipitation of carbides of Widmanstätten morphology at the prior austenite grain boundaries. Ferrite will form surrounding these carbides because carbon will be consumed for the carbide formation, triggering the formation of ferrite. The ferrite grows to a specific width and then, according to apt analysis, significant segregation of Cr and Mn is found at the α/α' (previously γ) boundary. It is therefore suggested that the coarsening of the ferrite ceases because of solute drag.

5. Conclusions

In the present study, bainite microstructures, which were produced by an isothermal treatment of 51CrV4 medium carbon, low alloy spring steel have been characterized by SEM TEM and APT. It was found that:

1. Bainitic ferrite contains more carbon in solution than is predicted from the thermodynamic equilibrium. The carbon content of the bainitic ferrite becomes higher as the transformation temperature decreases. This could be attributed to the possibletetragonality of bainitic ferrite, allowing higher solubility of C in α-Fe.
2. The substitutional alloying elements (Mn, Cr) did not partition to the carbides during lower bainite formation. Silicon was depleted from the carbides. This is a process occuring after the precipitation (tempering).
3. During upper bainite formation, segregation of Cr and Mn occurred at the cementite-bainitic ferrite interface.
4. A peculiar microstructure consisting of acicular carbides and ferrite formed at temperatures close to the bainite start temperature. It can be suggested based on the calculated thermodynamics that this microstructure is inverse bainite.
5. During inverse bainite formation, alloying elements can diffuse within the time frame of the transformation. APT measurements show that Mn and Cr partition to the boundaries of bainitic ferrite and into the carbides.
6. The difference in the chemical composition of the carbides in inverse bainite and the formation temperature can explain their presence and their morphology.

Acknowledgements

This research was performed under the project number M22.12.476 in the framework of the Research Program of the Materials innovation institute (M2i) (www.m2i.nl). M.H. Acknowledges funding from the German Federal Ministry of Education and Research (BMBF) through grant 03SF0535.

Data statement

The raw/processed data required to reproduce these findings cannot be shared at this time as the data also forms part of an ongoing study.

References

[1] A. Hultgren, Isothermal transformation of austenite, Trans. ASM 39 (1947) 815.
[2] M. Hillert, The Growth of Ferrite, Bainite and Martensite, Swedish Inst. for Metal Research, 1960.
[3] M. Hillert, Diffusion in growth of bainite, Metall. Mater. Trans 25A (1994) 1957–1966.
[4] C. Zener, Kinetics of the decomposition of austenite, Trans. ASM 167 (1946) 550–595.
[5] T. Ko, S.A. Cottrell, The formation of bainite, J. Iron Steel Inst. 172 (1952) 307.
[6] H.K.D.H. Bhadeshia, D.V. Edmonds, The mechanism of Bainite formation in steels, Acta Metall. 28 (1980) 1265–1273.
[7] R.K. Dutta, R.M. Huizenga, H. Gao, M. Amirthalingam, A. King, M.J.M. Hermans, I.M. Richardson, In-situ synchrotron diffraction studies on transformation strain development in a high strength quenched and tempered structural SteelPart I. Bainitic transformation, Metall. Mater. Trans. 45A (2014) 5281–5285 12 pp.
[8] C.N. Hulme-Smith, M.J. Peet, I. Lonardelli, A.C. Dippel, H.K.D.H. Bhadeshia, Further evidence of tetragonality in bainitic ferrite, Mater. Sci. Technol. 31 (2015) 254–256 2 pp.
[9] H. Goldenstein, J.A. Cifuentes, Overall kinetics and morphology of the products of austenite decomposition in a Fe-0.46 Pct C-5.2 Pct Cr alloy transformed isothermally above the bay, Metall. Mater. Trans. 37A (2006) 1747–1755.
[10] A. Borgenstam, P. Hedstrom, M. Hillert, P. Kolmskog, A. Stormvinter, J. Agren, On the symmetry among the diffusional transformation products of austenite, Metall. Mater. Trans. 42A (2011) 1558–1574.
[11] W.T. Reynolds, S.K. Liu, F.Z. Li, S. Hartfield, H.I. Aaronson, An investigation of the generality of incomplete transformation to bainite in Fe-C-X alloys, Metall. Trans. A.

21 (1990) 1479–1491.
[12] W.T. Reynolds, F.Z. Li, C.K. Shui, H.I. Aaronson, The incomplete transformation phenomenon in Fe-C-Mo alloys, Metall. Trans. 21 (1990) 1433–1463. A21.
[13] H.I. Aaronson, W.T. Reynolds Jr., G.R. Purdy, Coupled-solute drag effects on ferrite formation in Fe-C-X systems, Metall. Mater Trans A 35 (2004) 1187–1210.
[14] R. Kannan, Y. Wang, L. Li, A dilatometric analysis of inverse bainitic transformation, J. Mater. Sci. 55 (2018) 3692–3708.
[15] R. Kannan, Y. Wang, L. Li, Identification of inverse bainite in Fe-0.84C-1Cr-1Mn hypereutectoid low alloy steel, Metall. Mater. Trans. 48A (2017) 948–952.
[16] R. Kannan, Y. Wang, L. Li, A thermodynamic study of inverse bainite transformation, J. Mater. Sci. 53 (2018) 12583–12603.
[17] C. Goulas, M.G. Mecozzi, J. Sietsma, Bainite formation in medium-carbon low-silicon spring steels accounting for chemical segregation, Metall. Mater. Trans. 47A (2016) 3077–3087 6 pp.
[18] K. Thompson, J. Sebastian, S. Gerstl, Observations of Si field evaporation, Ultramicroscopy 107 (2007) 124.
[19] P.J. Felfer, T. Alam, S.P. Ringer, J.M. Cairney, A reproducible method for damage-free site-specific preparation of atom probe tips from interfaces, Microsc. Res. Tech. 75 (4) (2012) 484–491.
[20] S.K. Makineni, M. Lenz, P. Kontis, Z. Li, A. Kumar, P.J. Felfer, S. Neumeier, M. Herbig, E. Spiecker, D. Raabe, B. Gault, Correlative MicroscopyNovel methods and their applications to explore 3D chemistry and structure of nanoscale lattice defects: a case study in Superalloys, JOM 70 (2018) 1736–1743.
[21] M. Herbig, P. Choi, D. Raabe, Combining structural and chemical information at the nanometer scale by correlative transmission electron microscopy and atom probe tomography, Ultramicroscopy 153 (2015) 32–39.
[22] S.K. Makineni, A. Kumar, M. Lenz, P. Kontis, T. Meiners, C. Zenk, S. Zaefferer, G. Eggeler, S. Neumeier, E. Spiecker, D. Raabe, B. Gault, On the diffusive phase transformation mechanism assisted by extended dislocations during creep of a single crystal CoNi-based superalloy, Acta Mater. 155 (2018) 362–371.
[23] B. Gault, Advances in the calibration of atom probe tomographic reconstruction, J. Appl. Phys. 105 (3) (2009) 34.
[24] A.J. Clarke, M.K. Miller, R.D. Field, D.R. Coughlin, P.J. Gibbs, K.D. Clarke, D.J. Alexander, K.A. Powers, P.A. Papin, G. Krauss, Atomic and nanoscale chemical and structural changes in quenched and tempered 4340 steel, Acta Mater. 77 (2014) 17–27.
[25] Chen Zhu, X.Y. Xiong, A. Cerezo, R. Hardwicke, G. Krauss, G.D.W. Smith, Ultramicroscopy 107 (2007) 9 pp 808–812.
[26] J. Cornide, G. Miyamoto, F.G. Caballero, T. Furuhara, M.K. Miller, C. García-Mateo, Distribution of dislocations in nanostructured bainite, Solid State Phenom. 172-174 (2011) 117–122.
[27] I.B. Timokhina, K.D. Liss, D. Raabe, K. Rakha, H. Beladi, X.Y. Xiong, P.D. Hodgson, Growth of bainitic ferrite and carbon partitioning during the early stages of bainite transformation in a 2 mass% silicon steel studied by in situ neutron diffraction, TEM and APT, J Appl. Crystall. 49 (2016) 399–414.
[28] C. Goulas, Development of Novel Heat Treatments for Automotive Spring Steels: Phase Transformations Microstructure and Performance, Delft University of Technology, 2018, https://doi.org/10.4233/uuid:ce01998a-0830-494e-a403-9f0696aa0dce.
[29] A.A. Kaya, D.V. Edmonds, Nonclassical decomposition products of austenite in Fe-C-Cr alloys, Metall Trans 29A (1988) 2913–2924.
[30] K.R. Kinsman, H.I. Aaronson, The inverse Bainite reaction in hypereutectoid Fe-C alloys, Metall. Trans 1A (1970) 1485–1488.
[31] H.J. Lee, G. Spanos, G.J. Shiflet, H.I. Aaronson, Mechanisms of the bainite (non-lamellar eutectoid) reaction and a fundamental distinction between the bainite and pearlite (lamellar eutectoid) reactions, Acta Metall. 36 (1988) 1129–1140.
[32] G. Spanos, H.S. Fang, D.S. Sarma, H.I. Aaronson, Influence of carbon concentration and reaction temperature upon bainite morphology in Fe-C-2 Pct Mn alloys, Metall. Trans. 21A (1990) 1391–1411.